

GRACE storage-runoff hystereses reveal the dynamics of regional watersheds

E.A. Sproles^{1,2,3}; S.G. Leibowitz⁴; J.T. Reager⁵; P.J. Wigington Jr^{4,6}; J.S. Famiglietti⁵; S.D. Patil⁷

*corresponding author: eric.sproles@gmail.com

¹ Oak Ridge Institute for Science and Technology, c/o National Health and Environmental Effects Research Laboratory, US Environmental Protection Agency, 200 SW 35th Street, Corvallis, OR, 97333, USA

² Current address: Centro de Estudios en Zonas Áridas, Universidad de La Serena, Raul Bitran 1305, La Serena, Chile

³ College of Earth, Ocean, and Atmospheric Sciences, Oregon State University, Corvallis, OR, 97331-5503, USA

⁴ National Health and Environmental Effects Research Laboratory, US Environmental Protection Agency, 200 SW 35th Street, Corvallis, OR, 97333, USA

⁵ Jet Propulsion Laboratory, California Institute of Technology, Pasadena, California, 91109, USA

⁶ Retired

⁷ School of Environment, Natural Resources and Geography, Bangor University, Bangor, LL57 2UW, Wales

1 **Abstract**

2 We characterize how regional watersheds function as simple, dynamic systems through a
3 series of hysteresis loops using measurements from NASA's Gravity Recovery and Climate
4 Experiment (GRACE) satellites. These loops illustrate the temporal relationship between
5 runoff and terrestrial water storage in three regional-scale watersheds ($>150,000 \text{ km}^2$) of
6 the Columbia River Basin, USA and Canada. The shape and size of the hysteresis loops are
7 controlled by the climate, topography, and geology of the watershed. The direction of the
8 hystereses for the GRACE signals move in opposite directions from the isolated
9 groundwater hystereses, suggesting that regional scale watersheds require soil water storage
10 to reach a certain threshold before groundwater recharge and peak runoff occur. The
11 subsurface water (soil moisture and groundwater) hystereses more closely resemble the
12 storage-runoff relationship of a soil matrix. While the physical processes underlying these
13 hystereses are inherently complex, the vertical integration of terrestrial water in the
14 GRACE signal encapsulates the processes that govern the non-linear function of regional-
15 scale watersheds. We use this process-based understanding to test how GRACE data can be
16 applied prognostically to predict seasonal runoff (mean Nash-Sutcliffe Efficiency of 0.91)
17 and monthly runoff during the low flow/high demand month of August (mean Nash-
18 Sutcliffe Efficiency of 0.77) in all three watersheds. The global nature of GRACE data
19 allows this same methodology to be applied in other regional-scale studies, and could be
20 particularly useful in regions with minimal data and in trans-boundary watersheds.

21

22 1. Introduction

23 At the most fundamental level, watershed processes can be described as the
24 collection, storage, and release of water (Black, 1996; McDonnell et al., 2007). The runoff
25 from these processes is governed by threshold mediated relationships across scales that
26 result in storage—runoff hystereses (Spence, 2010). These threshold relationships between
27 storage and runoff (S — R) are not uniform across a watershed, functioning as a series of
28 discontinuous processes in soils and hillslopes that provide an integrated S — R relationship
29 at the watershed scale (Spence, 2010). Kirchner (2009) described the S — R relationship to
30 be non-linear and stated that watersheds typically function as dynamic systems governed by
31 their unique climate and geology. These conceptual models of hydrologic behaviors help
32 provide a process-based understanding of watersheds as dynamic environmental systems
33 (Aspinall, 2010), and identify connections that advance hydrologic science and hydrologic
34 prediction (Wagener et al., 2007).

35 At the local scale, *in situ* instrumentation can quantify the non-linear relationship
36 between streamflow and water stored in a watershed as snow, soil moisture, groundwater
37 and reservoirs (Appleby, 1970; Brutsaert, 2008; Kirchner, 2009; Sayama et al., 2011).
38 These four primary storage components, along with climate, topography, and geology
39 govern the fluxes of water through a catchment, and play an important role in the hysteretic
40 nature of storage and runoff dynamics (McGlynn and McDonnell, 2003; McNamara et al.,
41 2011). Knowledge of these processes is fundamental to developing an understanding of a
42 watershed’s hydrologic behavior. However, observations over larger regions can be
43 technically challenging and costly, and *in situ* measurements from small basins do not
44 necessarily represent the complexity inherent to watersheds at more broad scales (Spence,

45 2010). This scaling problem limits our capacity to understand and predict regional
46 hydrologic processes, which is often the practical scale of watershed management (Blöschl,
47 2001; Western et al., 2002; Skøien et al., 2003; Peel and Blöschl, 2011; Thompson et al.,
48 2011).

49 In the absence of broad-scale observations, past hydrological studies have typically
50 relied on *in situ* measurements as a proxy for regional scale hydrological processes. For
51 example, in higher latitude or mountainous regions measurements of snow water storage
52 have provided a simple metric that has been used in water resource planning for decades
53 (Cayan, 1996; United States Army Corps of Engineers, 2001), and are often correlated to
54 streamflow gauged downstream (Dozier, 2011). While informative, this approach can often
55 provide hydrological forecasts that are misleading, because point-based measurements do
56 not fully represent the broad-scale variability of rugged mountain terrain (Dozier, 2011;
57 Nolin, 2012; Webster et al., 2014; Ayala et al., 2014). Similarly, measurements of soil
58 moisture in the upper 2000 mm of the soil rely on point-based data that are often distributed
59 at the regional scale, but do not effectively represent the true variability of soil moisture
60 found at the regional scale (Western et al., 2002; Brocca et al., 2010). A complete
61 understanding of groundwater stores and fluxes (deeper than 2000 mm) at regional scales
62 also remains elusive, despite its increasing importance in water resources management
63 (Wagener et al., 2007; Gleeson et al., 2012; Famiglietti and Rodell, 2013; Barthel, 2014). In
64 addition to contributing to runoff, groundwater serves as an important water resource for
65 consumptive use (Gleeson et al., 2012).

66 While local-scale methods have been applied with moderate success in the past,
67 current trends in climate and in consumptive water demand suggest that long-term changes

68 in hydrological fluxes will have a major impact at the regional scale (Milly et al., 2008). As
69 a result, the supply and demand of water is also expected to shift, especially at the regional
70 scale (Wagner et al., 2010; Gleick, 2014a).

71 Hydrologic models can help address the questions of scale and bridge the gap
72 between local scale observations and regional-scale processes by estimating the primary
73 components of water storage (snow, soil moisture, reservoir, and groundwater) across a
74 larger spatial grid. Regional-scale modeling approaches are integrated into water resource
75 management operations for navigation, human consumptive use, irrigation, and hydropower
76 (Payne et al., 2004; Rodell et al., 2004). Models can also be applied diagnostically to test
77 scientific hypotheses and provide a better understanding of the physical processes that
78 govern real world systems, such as the connections between snowmelt, streamflow, and
79 groundwater (Beven, 2007, 2010; Moradkhani and Sorooshian, 2008; Kirchner, 2009;
80 Clark et al., 2011; Capell et al., 2012). Despite their utility, developing and validating a
81 model can be both time consuming and reliant on multiple data inputs, which even in the
82 most well-instrumented basins provides sparse geographic coverage (Bales et al., 2006;
83 Zang et al., 2012). The lack of an integrated measurement of water storage and streamflow
84 has limited regional-scale hydrologic insights to model-based studies (Koster et al., 2010;
85 Mahanama et al., 2011).

86 Since 2002, broad-scale measurements of changes in the amount of water stored
87 across and through the earth have been available from NASA's Gravity Recovery and
88 Climate Experiment (GRACE) satellites (Tapley et al., 2004). GRACE measures monthly
89 changes in the Earth's gravitational field that are proportional to regional changes in total
90 water storage (Wahr et al., 2006). GRACE satellites provide a monthly record of terrestrial

91 water storage anomalies (*TWSA*), which represent the changes in the vertical sum of water
92 at the Earth's surface stored in snow, surface, soil and groundwater. Water losses to runoff
93 and evapotranspiration are implicit in the GRACE storage signal, removing the added layer
94 of complexity typically required to model the terrestrial water balance.

95 GRACE data, coupled with modeled and measured variations of water stored in
96 snow, surface reservoirs and soils, have successfully been decomposed to quantify regional
97 groundwater changes (Rodell et al., 2009; Famiglietti et al., 2011; Voss et al., 2013; Castle
98 et al., 2014) and have contributed to improving water balance calculations (Zaitchik et al.,
99 2008; Li et al., 2012). More recent efforts have quantified the relationship between regional
100 water storage and specific streamflow events (Reager and Famiglietti, 2009; Reager et al.,
101 2014). Riegger and Tourian (2014) coupled GRACE data using data-driven and model-
102 based approaches to better understand the relationship between storage and runoff across
103 climatic zones globally. Their study found that coupled liquid storage is linear to runoff,
104 and that in climatic regions with snow and ice the relationship between storage and runoff
105 is more hysteretic. These novel analyses, which are more diagnostic in nature, have
106 provided new insights into regional watershed hydrology using GRACE measurements as a
107 core data input. These studies have not explored how topography and geology can also help
108 describe the $S-R$ relationship of regional watersheds. Nor did these studies examine the
109 ability of GRACE measurements to predict seasonal runoff.

110 In this paper, we use terrestrial water storage data from GRACE to better
111 understand the hydrology of regional watersheds and the relationship between storage and
112 runoff. The temporal relationships between coincident *TWSA* and discharge observations at
113 three scales in the Columbia River Basin (CRB) of western North America are investigated

114 using climate, topography, and geology as a framing principle to describe the shape of the
115 storage-streamflow hysteresis. We associate regional and temporal differences in the
116 hystereses with varying watershed dynamics. Finally, we compare the prognostic abilities
117 of GRACE observations with individual modeled estimates of snow and soil moisture to
118 predict seasonal streamflow at regional scales.

119 **2. Study Area**

120 Our study area is the Columbia River Basin (CRB; 41-53°N and 110-122°W; Fig.
121 1). This basin has dry summers and wet winters. Up to 70% of annual precipitation falls
122 between November and March, 50-60% of which occurs as snow (Serreze et al., 1999;
123 Nolin et al., 2012). The spring months (April to June) are also wet, but warmer.
124 Precipitation during the spring combines with snowmelt to swell rivers and potentially
125 exacerbate flooding. Snowmelt also serves as a critical component of the hydrologic cycle,
126 recharging aquifers and filling streams later in the year. These contributions bridge the
127 temporal disconnect between wet winters and dry summers when demand is at its peak as
128 farmers, fish, hydropower and municipal users vie for over-allocated water resources
129 (United States Army Corps of Engineers, 2001; Oregon Water Supply and Conservation
130 Initiative, 2008). However, concerns with winter surplus and summer scarcity are not
131 uniform across the CRB, since climate and geology vary greatly. Two of the study
132 watersheds, the Upper Columbia (155,000 km²) and the Snake River basin (182,000 km²),
133 represent distinctly different climatic, topographic, and geologic provinces of the CRB
134 (described and illustrated in Fig. 1). The Upper Columbia is wet and is characterized by
135 steep topography of fractured rock and poor groundwater storage. In contrast, the arid
136 Snake River basin is bowl-shaped with mountains on three sides. The interior of the Snake

137 River basin is a broad plain with well-developed soils and expansive aquifer storage. The
138 Columbia River at The Dalles (614,000 km²) encompasses the Upper Columbia and the
139 Snake River sub-basins, and its climate and geology are an integration of the two (Fig. 1).
140 A distinct climatic feature of the Columbia River at The Dalles is the western slope of the
141 Cascade Mountains, where over 3000 mm of mean annual precipitation at higher elevations
142 sustains a considerable seasonal snowpack. The scale of this study was constrained to
143 watersheds larger than 150,000 km², the optimal minimum geographic limit of GRACE
144 data (Yeh et al., 2006; Landerer and Swenson, 2012).

145 **3. Methods and Data**

146 We used 108 months of GRACE and streamflow data over nine water years (WY;
147 Oct – Sep; 2004–2012). This data comprises positive, neutral, and negative phases of the El
148 Niño-Southern Oscillation and negative and positive phases of the Pacific Decadal
149 Oscillation (Feng et al., 2014; Iizumi et al., 2014). As a result, the data provides years of
150 above- and below-average precipitation, snowpack, and streamflow for the region. The
151 three watersheds were delineated upstream from United States Geological Survey (USGS)
152 stream gages at 1° resolution, which is the resolution of GRACE data. In the CRB, these
153 grid cells represent a dimension of approximately 80 km by 120 km. The Upper Columbia
154 consists of the area upstream of the Columbia River at the International Boundary gage
155 (USGS 12399500), just downstream of the confluence of the Columbia and Pend-Oreille
156 Rivers. The Pend-Oreille is a major watershed in the upper portions of the CRB. The Snake
157 River gage at Weiser (USGS 13269000) provides gauged streamflow data above Hell’s
158 Canyon Reservoir, the largest impoundment in the Snake River basin. The USGS gage at
159 The Dalles (USGS 14105700) provides the most downstream streamflow data for the CRB.

160 Monthly mean runoff (R ; mm) was calculated for each of the three gages using the USGS
161 streamflow data.

162 Measurements of $TWSA$ were obtained from the GRACE RL-05 (Swenson and
163 Wahr, 2006; Landerer and Swenson, 2012) data set from NASA's Tellus website
164 (<http://grace.jpl.nasa.gov>). The errors present in the gridded GRACE data exist primarily as
165 a result of truncation (i.e., a low number of harmonics) in the spherical harmonic solution,
166 and smoothing and systematic noise removal (called "de-stripping") that is applied after
167 GRACE level-2 processing to remove spatially correlated noise (called "stripes") (Swenson
168 and Wahr, 2006). This smoothing tends to smear adjacent signals together (within the
169 radius of the filtering function), resulting in smaller signals being lost, and larger signals
170 having a coarser footprint and a loss of spatial information.

171 To restore the GRACE signal lost during processing, the data were scaled using 1°
172 Land-Grid Scale Factors produced by putting a 1° land surface model through identical
173 processing (truncation and filtering) as the GRACE solutions, then measuring the decrease
174 in the signal amplitude at each 1° grid. These procedures are described on the Tellus
175 website and detailed in Landerer and Swenson (2012). Monthly 1° GRACE estimates of
176 $TWSA$, and the associated 1° leakage and measurement errors, were spatially averaged over
177 each of the three study watersheds following the procedures described in the Tellus
178 website.

179 GRACE represents monthly storage anomalies relative to an arbitrary record-length
180 mean value, analogous to the amount of water above or below the long-term mean storage
181 of a bucket, and should balance with the equation:

182
$$\Delta Storage = TWSA = \Delta GW + \Delta SM + \Delta SWE + \Delta RES \quad (1)$$

183 where all components are at monthly time steps; *GW* represents groundwater, *SM*
184 represents soil moisture (from 0–2000 mm depth), *SWE* represents snow water equivalent
185 (the equivalent depth of water held in snowpack), and *RES* represents reservoir storage. The
186 Δ used here represents the anomaly from the study-period mean, rather than a monthly
187 change. To isolate monthly groundwater storage anomalies ($\Delta GW = GWSA$) in the above
188 equation, ΔSM , ΔSWE and ΔRES estimates were subtracted from the monthly *TWSA* data
189 using methods described in Famiglietti et al. (2011). Similarly, the combined signal of
190 water storage anomalies of subsurface moisture ($TWSA_{sub}$), *SM* and *GW*, was isolated by
191 subtracting *SWE* and *RES* from *TWSA* values.

192 Monthly *SM* values over the study basins were obtained from the mean of the North
193 American and Global Land Data Assimilation Systems (NLDAS at 1/8° resolution
194 (Cosgrove et al., 2003) and GLDAS at 1/4° resolution (Rodell et al., 2004), respectively),
195 and were spatially averaged over the three study watersheds. Monthly 1-km resolution *SWE*
196 values were obtained from the mean of NLDAS and Snow Data Assimilation System
197 (SNODAS; National Operational Hydrologic Remote Sensing Center, 2004) and were
198 spatially averaged over the three watersheds. SNODAS data were used in place of the
199 GLDAS data product, which considerably underestimated *SWE* in mountainous areas when
200 compared to point-based measurements. Changes in monthly reservoir storage were
201 calculated for the five largest reservoirs in the CRB (see Table A1). Other smaller
202 reservoirs in the CRB were excluded when it was determined that fluctuations in their
203 levels were below the detection limits of GRACE.

204 Like all measurements, estimates of *TWSA* from GRACE contain error. For all of
205 the study basins, the range of error is well below the *TWSA* signal strength, approximately
206 an order of magnitude below the annual amplitude (200 – 300 mm) of the *TWSA* signal in
207 the CRB. The basin-averaged *TWSA* errors (time invariant) for the three study basins are 37
208 mm (Upper Columbia), 22 mm (Snake), and 25 mm (The Dalles).

209 The model data from LDAS and SNODAS simulations are driven by *in situ*
210 measurements, and represents the best available data for broad scales. We address any
211 structural error from an individual model by using an ensemble of outputs. Calculation of
212 the error in individual terms followed standard methodologies (Famiglietti et al., 2011),
213 where error in *SM* is the mean monthly standard deviation, and standard errors for *SWE* and
214 *RES* are 15% of mean absolute changes. *GWSA* and *TWSA_{sub}* anomaly errors are
215 calculated as the sum of basin-averaged errors (added as variance) in the individual terms in
216 each respective calculation (eq. 1), including the error in *TWSA* (Swenson et al., 2006). The
217 basin-averaged error variance for *GWSA* (time invariant) in the three study basins are 45
218 mm (Upper Columbia), 26 mm (Snake), and 33 mm (The Dalles). For *TWSA_{sub}* these
219 values are 37 mm (Upper Columbia), 22 mm (Snake), and 25 mm (The Dalles). The
220 individual error components (*SM*, *SWE*, *RES* respectively) for each basin are Upper
221 Columbia (24 mm, 6 mm, 0.01 mm), Snake (14 mm, 3 mm, 0.01 mm), and The Dalles (21
222 mm, 4 mm, 0.01mm). Note that these error estimates are distributed across an entire
223 regional watershed and do not represent the error at individual monitoring sites. A time
224 series of these values and basin-averaged errors is provided in Fig. 2.

225 Based on an approach similar to Reager et al. (2014) and Riegger and Tourian
226 (2014), we plotted the temporal relationship between *TWSA* and *R* to examine hysteresis

227 relationships in all three of the study watersheds for each individual water year and for the
228 monthly mean across all water years. Expanding from the integrated terrestrial component
229 of water storage, we also plotted the relationships of $TWSA_{sub}$ and $GWSA$ with R . We
230 examined the branches of these hysteresis plots to better understand how the size, shape,
231 and direction of the hystereses varied across years in each of the three regional watersheds.

232 In order to verify groundwater hysteresis, we compared the GRACE-derived $GWSA$
233 to groundwater depths from well measurements at 33 sites throughout the study region
234 (Fig. 1 and Table A2). These data were normalized by their standard deviation, and the
235 mean of the 33 wells was calculated. The standard deviation of the GRACE-derived $GWSA$
236 for The Dalles was normalized to provide a direct comparison of $GWSA$ and *in situ*
237 measurements.

238 We further hypothesized that because peak SWE accumulation occurs between
239 February and April, that $TWSA$ for these months could be used to predict R for an
240 individual month and the cumulative seasonal runoff (R_{season}) that occurs after peak SWE
241 accumulation. To test this prognostic hypothesis we used a two-parameter power function
242 (The MathWorks, 2013):

$$243 \quad R_{predicted} = a(TWSA_{month})^b + c \quad (2)$$

244 where $R_{predicted}$ is runoff for the predicted time interval; $TWSA_{month}$ represents terrestrial
245 water storage for an individual month, and a , b , and c are fitted parameters from the power
246 function.

247 We tested this relationship for $TWSA$ in February, March and April to predict R_{season}
248 (April – September) and for the individual months of July (R_{July}), August (R_{Aug}), and

249 September (R_{Sep}); these represent the lower-flow months when demand is near its peak.
250 Additionally, we tested and compared the modeled-values of SWE from NLDAS and
251 SNODAS and SM from NLDAS and GLDAS, and the model-derived values of $TWSA_{\text{sub}}$ to
252 predict R_{season} and for the individual months using the same power-function analysis.

253 Because our data set was constrained to nine water years, we used a double-pass
254 approach to fit and test the empirical relationship between S — R . This approach allowed us
255 double our data inputs for calculating standard hydrologic evaluation metrics such as Root
256 Mean Square Error (RMSE), Nash-Sutcliffe Efficiency (NSE) and Coefficient of
257 Determination (R^2); (Legates and McCabe, 1999). The nine years were divided into two
258 sets (Set 1, even years 2004-2012; Set 2, odd years 2005-2011). The first pass calculated
259 the power function of S — R to Set 1, and the parameters were then tested against Set 2. The
260 roles of the datasets were then reversed, and the empirical model results of each pass were
261 compiled into one data set and tested against measured values to calculate RMSE, NSE,
262 and R^2 . In order to maximize the limited data inputs, once we tested the two independent
263 sets for model performance, we combined the data sets for a single power function curve.
264 The observed data were tested against the simulated data from the complete, but limited
265 data record. The final model curve was fit to these data.

266

267 **4. Results**

268 **4.1. Storage-runoff hysteresis**

269 The filling and emptying of the study basins at the regional-scale over the course of
270 an individual WY results in a hysteretic relationship between storage and runoff (Fig. 3a).

271 The hysteresis loops begin at the onset of the wet season in October, with *TWSA* increasing
272 (Figs. 3a, 4a-c) as precipitation is stored as snow and soil moisture. An increase in storage
273 that is not offset by an increase in discharge indicates a predominance of snow inputs and
274 the freezing of soil water. The lower branch of the hysteresis plot (storage increase
275 unmatched by runoff) can be used to estimate cumulative snow water equivalent and soil
276 moisture in the basin. This is the water that later contributes to streamflow and groundwater
277 recharge in the spring.

278 The hysteresis shifts direction from Feb-Apr (inflection 1, Fig. 3a) when saturated
279 soils and snowmelt cause *R* to rapidly increase. Each hysteresis loop contains a vertical
280 branch of the curve during which storage is relatively constant, but streamflow increases
281 rapidly. This also represents the groundwater recharge branch of the loop. As snow melts
282 and the ground thaws, runoff is generated, recharge into soils occurs, and basins tend to be
283 at peak storage during this branch. Storage losses and additional precipitation inputs during
284 this period are re-organized internally. A second shift (inflection 2, Fig. 3a) occurs from
285 Apr-June when peak *TWSA* begins to decrease, representing spring snowmelt and a switch
286 from precipitation that falls primarily as snow to rain; these combine to contribute to peak
287 *R*.

288 Once peak *R* values are reached, the loop shifts direction a third time (inflection 3,
289 Fig. 3a), receding on both axes as contributions from snowmelt diminish while presumably
290 groundwater sustains streams and provides a source for irrigated agriculture. During this
291 period, the relationship between *TWSA* and discharge is more linear, corresponding to
292 baseflow-driven runoff processes in which each monthly change in storage causes a
293 proportional change in the generation of streamflow.

294 The hysteresis plots of $TWSA$ — R for an individual water year demonstrate that the
295 timing and quantity of precipitation governs the size of a hysteresis loop for an individual
296 WY (Figs. 3a, 4a-c, 5). For instance wet years (e.g., 2008) have bigger loops, while dry
297 years (e.g., 2005) are more compressed along both axes. However, the general shape of the
298 loops is distinct for each basin. Plotting multiple WYs provides a family of curves for each
299 basin that helps describe how climate, topography, and geology govern the timing and
300 magnitude of the relationship between $TWSA$ and R (Figs. 3a, 5).

301 **4.2. Subsurface water ($TWSA_{sub}$) – runoff hysteresis**

302 The $TWSA_{sub}$ hysteresis curve contracts horizontally when the snow signal is
303 removed from $TWSA$ values for both the Upper Columbia and The Dalles (Figs. 3b, 4d-f),
304 which collapses the loops and takes a form similar to a plot-scale hysteresis of soil. Peak
305 $TWSA_{sub}$ occurs in June, which corresponds to the spring melt of mountain snowpack and
306 the end of the wet season (Figs. 4d-f). However in the Snake River, the hysteresis curve
307 still retains a loop, but the timing of maximum $TWSA_{sub}$ is also earlier, reaching its peak
308 during March and April (Fig. 4e). It is noteworthy that in the Snake River the $TWSA_{sub}$ — R
309 hysteresis loop temporally progresses in the opposite direction, but stays in phase with
310 precipitation inputs.

311 **4.3. Groundwater-runoff hysteresis**

312 The hysteresis loops describing the temporal relationship between $GWSA$ and R are
313 equally informative, with one distinct difference—they temporally progress in opposite
314 directions of the hysteresis loops of $TWSA$ and R (Fig. 3). For all three watersheds, $GWSA$
315 decreases from Oct–Feb/Mar (Fig. 4h-j), which is out of phase with the onset of the wet

316 season. *GWSA* does not shift towards positive gains until early spring and the initial stages
317 of melt before reaching its maximum in June.

318 The 33 point-specific well data located across the CRB show considerable
319 individual variability throughout a water year, and the mean of the normalized standard
320 deviations of well levels was close to zero for all months. The temporal variability for the
321 well data provides no discernable correlation with the derived *GWSA* signal (Fig. A1).

322 **4.4. Individual basin hysteresis plots of *TWSA*, *TWSA_{sub}*, *GWSA* and *R***

323 Of the three study basins, the Upper Columbia is the most hydrologically active,
324 showing the largest annual range for *TWSA*, *TWSA_{sub}*, *GWSA*, and *R* (Fig. 6). The *TWSA*—*R*
325 hysteresis loops are more open (Fig. 4), corresponding to the fluxes of water moving
326 through watershed. When *SWE* is removed and subsurface water is highlighted, the
327 *TWSA_{sub}*—*R* hysteresis loops collapse horizontally and more closely resemble the
328 hystereses associated with soil (Figs. 4d). However the inter-annual range ($WY_{\max} -$
329 WY_{\min}) for *TWSA_{sub}* in the Upper Columbia is considerably greater than the other two
330 basins (median range = 234 mm; Fig. 6). As the hysteresis reverses directions for *GWSA*—
331 *R*, the loops shift to a more open shape (Figs. 4d), but the inter-annual range remains
332 similar.

333 In contrast to the rapid response of the Upper Columbia, the Snake River receives
334 ~60% less annual precipitation, but has an annual *TWSA* range that is only 22% less
335 (median annual range = 192 mm; $R=7$ mm; Figs. 4, 5, and 6). However, the *TWSA*
336 hysteresis loops for the Snake River are collapsed vertically (Fig. 4b). In the more arid
337 Snake River, removing the snow signal does not collapse the *TWSA_{sub}*—*R* hysteresis loops

338 ($TWSA_{sub} = 89$ mm). Similarly, the *GWSA* loops suggest that subsurface moisture plays a
339 more prominent role in the Snake River.

340 The climate, topography, and geology of the Columbia River at The Dalles are an
341 integration of the Upper Columbia and Snake River, seen in the shape of the hysteresis
342 loops (Figs. 4, 5, 6; median annual range $TWSA=195$ mm; $R=27$ mm). The period from
343 Feb–June more closely resembles the Snake River basin, with gradual increases in $TWSA$
344 and sharp increases in R . The slope of the recession from June-Sept has the same general
345 shape for The Dalles as the Upper Columbia (Figs. 4a, 4c), presumably from snowmelt-
346 generated runoff.

347 **4.5. Streamflow forecasting**

348 We next present how $TWSA$ was applied prognostically to predict streamflow.
349 Using the double-pass calibration and validation approach, $TWSA_{Mar}$ provided the best
350 overall predictive capabilities for R_{season} with a mean NSE (\overline{NSE}) and mean R^2 ($\overline{R^2}$) of 0.75
351 and 0.91, respectfully (Fig. 7a, Table 1), for all three basins. The Dalles had the highest
352 NSE and R^2 , and lowest RMSE values (0.98, 0.98, 6 mm; Table 1). The results in the
353 Upper Columbia were also robust (0.82, 0.86, 33 mm; Table 1), while the Snake River
354 performed with less skill (0.46, 0.59, and 14 mm, Table 1). Applying $TWSA_{April}$ also
355 provided similar results, but with a lower degree of skill in predicting R ($\overline{NSE} = 0.57$, $\overline{R^2} =$
356 0.69). $TWSA_{Apr}$ provided improved predicted capabilities in the Upper Columbia (0.87,
357 0.88, and 28 mm, Table 1), but inferior results in the other two watersheds. $TWSA_{Feb}$ had a
358 low degree of skill in predicting R in all three watersheds (Table A3).

359 $TWSA_{Mar}$ and $TWSA_{April}$ also served as a good predictor of monthly runoff in July
360 and August for the Upper Columbia and to a lesser degree in The Dalles (Tables 1 and A3).
361 In the Snake River, $TWSA$ did not serve as a good predictor for R in an individual month.

362 Snowpack and soil moisture play a considerable role in the hydrology of the CRB
363 and are commonly used to help predict water demand and availability later in the year
364 (Koster et al., 2010). We compared the capabilities of the modeled snow (SWE) and soil
365 moisture (SM) products to predict R to the skill of measured GRACE $TWSA$ data (Table 1).
366 In the Upper Columbia and The Dalles, $TWSA_{Mar}$ predicts seasonal and monthly runoff
367 (July and August) with considerably more skill than SWE or SM (Figure 7, Table 1). In the
368 Snake River, SM_{Mar} has a higher degree of skill than $TWSA_{Mar}$ in predicting R_{season} and R_{Aug} .
369 SWE_{Mar} provided inferior results in all three watersheds, but with some predictive skill in
370 the Upper Columbia and The Dalles (NSE of 0.24 and 0.46 respectively, Table 1). In all
371 three watersheds, $TWSA_{sub}$ provided extremely poor predictions (Tables 1 and A3).

372 When the results of the empirical model using two independent sets of data proved
373 robust for some of the storage metrics, the observed data were tested against the simulated
374 data from the complete, but limited data record. The performance of the empirical model
375 improved using the complete data set (Tables 2 and A4), with the same general results.
376 $TWSA_{Mar}$ provided the best model fit for seasonal runoff in the Upper Columbia (NSE =
377 0.93, RMSE = 19.8 mm) and The Dalles (NSE = 0.98, RMSE = 5.7 mm). In the Snake
378 River, predictive capabilities improved more dramatically (NSE = 0.83, RMSE = 7.4 mm),
379 but soil moisture still served as a better predictor of seasonal streamflow (NSE = 0.93,
380 RMSE = 5.2 mm). Similarly, $TWSA_{Mar}$ provided the best model fit for runoff in August,
381 one of the drier months when demand is at its peak (Tables 2 and A4).

382 5. Discussion

383 5.1. Storage-runoff hysteresis

384 Decades of data collection and monitoring at individual gage sites indicate that
385 watersheds collect, store and release water. Using one integrated measurement from the
386 GRACE satellites, our results show these same process at the regional scale in the
387 hysteresis loops of storage (*TWSA*) and runoff (*R*). While hystereic processes have
388 previously been identified in local-scale measurements (McDonnell, 2003; McGlynn and
389 McDonnell, 2003), only recently has streamflow-storage hysteresis been identified at the
390 regional scale (Riegger and Tourian, 2014).

391 Our work builds on Riegger and Tourian's (2014) results, and employs GRACE data to
392 describe how regional watersheds function as integrated, non-linear systems governed by
393 climate, topography, and geology. Climate controls the size of the hysteresis loops by
394 providing a first-order control on hydrologic inputs and the storage of solid water, which in
395 turn governs the ranges of *TWSA* and *R*. However, runoff response to precipitation and
396 snowmelt does not act independently from topography and geology (Jefferson et al., 2008;
397 Tague et al., 2008), which controls how liquid water is stored and routed through a
398 watershed, even at the regional scale. The climatic, topographic, and geological
399 characteristics of each watershed provide an explanation of the *S—R* relationship that helps
400 govern the shape and size of its respective hysteresis curve. GRACE offers a single,
401 integrated measurement of changes in water storage through and across a watershed that
402 can be applied to predict regional streamflow using an empirical model. Where these

403 predictive capabilities succeed and fail help better describe the climatic, topographic, and
404 geological characteristics in each watershed.

405 For example, in the Upper Columbia, steep topography and wet climate fills subsurface
406 storage quickly before reaching a threshold in April or May. After this watershed-scale
407 threshold is reached, the steep topography moves snowmelt and rain quickly through the
408 terrestrial system and into the river channel until cresting in June (Figs. 4, 5, and 6),
409 followed by declines in $TWSA$ and R from June-September. These large fluxes of water
410 create a more open hysteresis loop, expanding non-linearly on both the horizontal and
411 vertical axes.

412 The Upper Columbia also has the broadest range of annual $TWSA_{sub}$ and $GWSA$ during
413 the study period (Figs. 5 and 6), despite having limited aquifer capacity. Conceptually, this
414 demonstrates that the upper limit of storage is greater than in the Snake River or The
415 Dalles, but that it also loses the most water. Its minimums at the end of the WY are also the
416 lowest (median $TWSA_{Sep} = -98\text{mm}$; Figs. 5 and 6). This range across $TWSA$, $TWSA_{sub}$, and
417 $GWSA$ supports the conceptual model that the watershed fills during the wet season, and is
418 then drained more quickly due to steep topography and limited water storage. The
419 predictive capability of $TWSA$ also strongly suggests that the components and temporal
420 relationships of storage across this watershed are interconnected, and that incorporating
421 April snowpack improves the model results.

422 In contrast, the arid Snake River basin provides a very different family of hysteresis
423 curves (Figs. 4, 5) that identify groundwater and soil moisture as primary components of
424 watershed function. The curves are compressed vertically (R) as compared to the Upper

425 Columbia, and are more constrained horizontally (Fig. 6). The onset of spring melt runoff
426 in February does not deplete $TWSA$ for the Snake River. Instead, $TWSA$ continues to
427 increase until May, when peak runoff occurs. As $TWSA$ decreases to the end of the water
428 year in September, the median $TWSA_{Sep}$ measurement (-78 mm) is 20 mm greater than in
429 the Upper Columbia. This indicates that the lower drainage threshold of the Snake River
430 watershed is relatively greater than the Upper Columbia, potentially explained by a less
431 severe topography and higher aquifer capacity.

432 The $TWSA_{sub}$ hysteresis curves in the Snake River retain a similar shape to the
433 $TWSA$ signal. While they reverse direction they do stay temporally connected to the onset
434 of the wet season in October, indicating that subsurface moisture is a central control on the
435 filling of the watershed through May. The capabilities of SM to empirically predict R better
436 than $TWSA$ further highlight the importance of subsurface water in this watershed. The
437 intra-annual range of $GWSA$ in the Snake River is also more limited than in the more
438 hydrologically responsive Upper Columbia. This more limited range of data supports the
439 conceptual model of a watershed that retains comparatively more winter precipitation in
440 soils and aquifers throughout the spring season, and that sustains flow later in the year and
441 until the onset of melt the following winter.

442 The greater Columbia River Basin upstream from The Dalles integrates the climatic,
443 topographic, and geologic characteristics of the Snake River and Upper Columbia as well
444 as other areas within the CRB. The western slope of the Cascades (Fig. 1), which is outside
445 of the Upper Columbia, accumulates up to several meters of SWE each winter. Due east of
446 the Cascades, an expansive basalt plain that provides aquifer storage helps dampen the

447 snowmelt pulse in the spring. The hysteresis loops for The Dalles reflect these combined
448 characteristics.

449 Storage at The Dalles increases along the horizontal axis ($TWSA$) until peak storage
450 is reached in March or April (Figs 3, 4, and 5). This $TWSA$ threshold responds with an
451 increase in R that continues through June. In July, the hysteresis begins to recede along
452 both axes closing out the loop. The $GWSA$ has the most limited range, potentially explained
453 by the extensive basalt aquifer moderating the relationship between storage and runoff. In
454 The Dalles, $TWSA_{Sep}$ has a median value of -88mm (Fig. 6), between the lower drainage
455 thresholds of the Upper Columbia and Snake River watersheds; indicating an integration of
456 the contributing climate, topography, and geology.

457 **5.2. Distinguishing the difference between $TWSA_{sub}$ and $GWSA$**

458 Conceptually $TWSA_{sub}$ represents changes in the amount of water stored as soil
459 moisture and groundwater, where as $GWSA$ represents water changes greater than 2000mm
460 below the soil surface. The goals of evaluating these metrics were to see if monthly changes
461 in soil moisture were linked to changes in groundwater storage, and the role of snowpack in
462 the S — R relationship.

463 The $TWSA_{sub}$ hysteresis curves in the Upper Columbia and The Dalles collapse into
464 a more linear relationship that is more commonly associated with the S — R relationship of a
465 soil matrix (Fig. 3 and 4). This is in contrast to the $GWSA$ hystereses that are represented by
466 loops that show an out-of-phase relationship between precipitation and groundwater
467 recharge from the start of the wet season in October until February or March. The $TWSA_{sub}$
468 and $GWSA$ hysteresis plots demonstrate that in these two basins changes in monthly soil

469 moisture are not always temporally aligned with *GWSA*. This can be explained by the
470 physical reality that soil moisture and groundwater are not always interconnected, and that
471 there is not a fixed depth (i.e., 2000 mm) that separates the two components of water
472 storage.

473 GRACE-derived calculations of *GWSA* also provide insights into the hydrological
474 processes governing groundwater recharge and depletion, as evidenced in the *GWSA*
475 hysteresis loops. The *GWSA—R* curves show an out-of-phase relationship between
476 precipitation and groundwater recharge from the start of the wet season in October until
477 February or March. This indicates that groundwater helps sustain stream flow during the
478 wet fall and winter and that pore space in soils and geologic materials must fill to a certain
479 threshold before groundwater begins to recharge and runoff is generated. The relationship
480 between the *TWSA* and *GWSA* curves from Oct-Mar identifies how the onset of snowmelt
481 also marks the beginning of groundwater recharge, and suggests that snowmelt inputs to
482 groundwater are considerable. In the CRB this is critical as current climate trends are
483 projected to reduce snowpack accumulation and exacerbate melt in the region (Wu et al.,
484 2012; Rupp et al., 2013; Sproles et al., 2013).

485 Additionally, our analysis identifies summer as the time of peak groundwater
486 storage in all three regional watersheds. This finding is of value for groundwater
487 management and policy decisions, as peak groundwater levels in June correspond to the
488 timing of groundwater pump tests that are used to develop groundwater withdrawal
489 regulations (Jarvis, 2011, 2014). Our data suggest that groundwater pump tests should not
490 be limited to an individual month, and should also include periods of reduced storage
491 particularly during the winter months. The inclusion of multiple pump tests throughout the

492 year could be particularly relevant as the population and water demand is projected to
493 increase in the region.

494 The point-specific well data are not conclusive and show considerable variability
495 with no consistent pattern regarding the timing of recharge and peak groundwater levels.
496 This is presumably a function of how site characteristics (i.e., usage, depth, location,
497 elevation) are extremely variable across a region. Rather than excluding these results or
498 selecting individual wells that match GRACE data, we discuss the results from all 33 wells
499 to help demonstrate the high variability that exists from well to well, and that
500 measurements of groundwater changes at a fixed location does not represent watershed-
501 scale characteristics (Jarvis, 2011, 2014). The disconnect between sites also highlights the
502 concept brought forward by Spence (2010), that storage is not uniform across a watershed,
503 and functions as a series of discontinuous processes at the watershed scale.

504 **5.3. Applying the S — R relationship as a predictive tool**

505 We applied these climatic, topographic, and geologic insights to develop and test
506 the hypothesis that spring $TWSA$ could predict R later in the year, based on two
507 observations: First, the shapes of the hysteresis curves for each basin are similar (Figs. 4a-c,
508 5), but vary by magnitude of annual $TWSA$. Second, peak $TWSA$ occurs before the peak
509 runoff. We show that the integrated GRACE signal is a good baseline measurement to
510 empirically predict seasonal streamflow across a range of water years with regards to
511 precipitation and streamflow. In essence, our data suggest that the water stored across and
512 through the Columbia River Basin in March describes the water available for the remainder
513 of the water year.

514 In the CRB and in the northwestern United States, peak snowpack occurs in March
515 or April, and is commonly used as a metric for predicting spring runoff. Despite the
516 importance of snowpack to the hydrologic cycle of the region, measurements of $TWSA_{Mar}$
517 from GRACE provide a better prediction of R_{season} , R_{July} , and R_{Aug} than model-derived
518 estimates of snowpack. GRACE $TWSA_{Mar}$ also provided a better prediction for runoff than
519 soil moisture, except for the Snake River watershed. There March soil moisture provided a
520 better indicator of runoff for the rest of the year. $TWSA_{Feb}$ provided inferior predictive
521 capacity, as the annual maximum $TWSA$ values have not been reached.

522 These results are promising with regards to using GRACE as a predictive tool for
523 water resources in both wet and dry years. Our limited data record represents a wide-range
524 of conditions with regards to climate and streamflow, which is captured in our empirical
525 models and is shown in the box plots to the right of Figs. 7a - b. These same results also
526 indicate that R is insensitive to $TWSA_{Mar}$ values below 100 mm. This lower threshold
527 describes with some certainty the amount of runoff that will be available for operations for
528 the remainder of the year.

529 We recognize that all three of these regional watersheds are managed through a
530 series of dams and reservoirs that create an altered runoff signal. Water resources managers
531 use point-specific and model-based estimates of water storage in the region to optimize
532 their operations for the water year. Additionally, in the fertile plains of the Snake River and
533 lower CRB, broad-scale agriculture relies on both ground- and surface water for irrigation.
534 Water withdrawals would be implicit in the $TWSA$ signal and reduce R . However, a more
535 detailed analysis of withdrawals lies outside the scope of this study.

536 Regardless of the length of record or anthropogenic influence, climate, topography,
537 and geology still provide the first-order controls on water storage that are found in the
538 hysteresis loops. GRACE encapsulates these hydrologic processes through measurements
539 of *TWSA*. The hysteresis loops expand and contract accordingly during wet and dry years,
540 as the intra-annual relationship between *TWSA* and *Q* represents the fluxes of water into
541 and out of the watershed. Despite intra-annual differences, a family of hysteresis curves can
542 describe each of the sub-regional watersheds. The predicative capability using *TWSA*, the
543 vertical sum of water, as compared to snowpack and soil moisture further highlights the
544 integrated nature of water storage in regional hydrology. These predictive capabilities
545 highlights the potential of GRACE to improve upon seasonal forecast predictions and
546 regional hydrological models.

547 **5.4. GRACE as an analysis tool for regional watersheds**

548 Where previous approaches to modeling watershed behavior have focused on
549 separate storage compartments, new approaches should include the magnitude and direction
550 of hysteresis (Spence, 2010). This integrated approach would provide new ways forward to
551 classify watersheds not only by runoff, but also on the first-order controls that govern the
552 non-linear hydrological processes.

553 Even though GRACE is somewhat of a blunt instrument with regards to temporal
554 (monthly) and spatial (1°) resolution, this emerging technology provides a new dimension
555 to regional watershed analysis by providing an integrated measurement of water stored
556 across and through the Earth. These measurements continue to prove their value in
557 retrospective analysis of regional hydrology (Rodell et al., 2009; Castle et al., 2014).

558 However, the hysteresis loops presented by Riegger and Tourian (2014) and further
559 developed in this paper demonstrate the ability of GRACE data to help develop a process-
560 based understanding of how regional watersheds function as simple, dynamic systems. As
561 the temporal record of GRACE continues to increase, its value as both a diagnostic and
562 predictive tool will continue to grow. In the mean time, these data have value in
563 augmenting existing management strategies.

564 Perhaps one of the most important facets of GRACE data is that it does not
565 distinguish political boundaries. It is not linked to a specific *in situ* monitoring agency with
566 limited data access and has the capacity to bridge sparse and inconsistent on-the-ground
567 hydrologic monitoring networks that exist in many regions of the world. Previous GRACE-
568 based analysis has shown its value in highlighting negative trends in terrestrial water
569 storage in trans-boundary watersheds (Voss et al., 2013; Castle et al., 2014), and resulting
570 regional conflict exacerbated by water shortages (Gleick, 2014b). GRACE provides an
571 objective measurement of a region's water resources that can provide valuable insights into
572 potential shortages or surpluses of water resources, and simple empirical predictions of
573 seasonal and monthly runoff that are easily deployable in places with limited data.

574 **6. Conclusions**

575 We have shown how GRACE-based measurements of *TWSA* distill the complexity
576 of regional hydrology into a simple, dynamic system. *TWSA* and derived estimates of
577 *GWSA* reveal hysteretic behavior for regional watersheds, which is more commonly
578 associated with hydrologic measurements at local scales. While the magnitude of the
579 hysteresis curves vary across years, they retain the same general shape that is unique to

580 each watershed. We demonstrated the utility of these hysteresis curves by showing how the
581 complete *TWSA* record during March and April can be used to empirically predict *R* for the
582 remainder for the water year ($TWSA_{Mar}$, mean NSE = 0.91) and during the drier summer
583 months ($TWSA_{Mar}$, mean NSE for July = 0.76, August = 0.72; Tables 1 and 2).

584 Because GRACE *TWSA* can augment prediction, managers could start to interpret
585 each year's hysteresis curve for the upcoming spring and summer, providing greater clarity
586 and validation for model-based forecasts presently used by water resource managers. Our
587 results demonstrate a way forward, expanding GRACE from a diagnostic tool, into a
588 conceptual model and predictive resource.

589 Although this study focused on the CRB, which has a rich data record, GRACE data
590 are available at a global scale and could be readily applied in areas with a paucity of data to
591 understand how watersheds function and to improve streamflow forecasting capabilities.
592 GRACE does not discern political boundaries and provides an integrated approach to
593 understanding international watersheds (Voss et al., 2013). This resource could serve as a
594 valuable tool for managers in forecasting surplus and scarcity, and in developing strategies
595 that include changes in supply and demand due to human consumptive needs and current
596 climate trends (Wagener et al., 2010; Gleick, 2014a).

597

598 **Author Contributions**

599 E.A.S., S.G.L., and P.J.W. developed the hysteresis concept based upon background
600 research by J.R. and J.S.F. The data analysis was led by E.A.S., but represents a combined
601 effort from all of the authors. J.R. provided expertise in the GRACE data product,
602 groundwater, and error analysis. E.A.S. prepared the manuscript with contributions from all
603 co-authors.

604 **Acknowledgments**

605 The authors would like to thank Matthew Rodell and Felix Landerer for their
606 expertise in understanding GRACE data during the initial stages of the research. GRACE
607 terrestrial data were processed by Sean Swenson, supported by the NASA MEaSUREs
608 Program, and are available at <http://grace.jpl.nasa.gov>. The GLDAS and NLDAS data used
609 in this study were acquired as part of the mission of NASA's Earth Science Division and
610 archived and distributed by the Goddard Earth Sciences Data and Information Services
611 Center. We would like to thank the reviewers of the manuscript that have helped improve
612 its overall quality. Additionally, Tim Kerr provided objective feedback and comments on
613 the research findings. The information in this document has been funded entirely by the US
614 Environmental Protection Agency, in part by an appointment to the Internship/Research
615 Participation Program at the Office of Research and Development, U.S. Environmental
616 Protection Agency, administered by the Oak Ridge Institute for Science and Education
617 through an interagency agreement between the U.S. Department of Energy and EPA. This
618 manuscript has been subjected to Agency review and has been approved for publication.

619 Mention of trade names or commercial products does not constitute endorsement or
620 recommendation for use.

621

622 **References**

- 623 Appleby, F. V.: Recession and the baseflow problem, *Water Resour. Res.*, 6(5), 1398–
624 1403, doi:10.1029/WR006i005p01398, 1970.
- 625 Aspinall, R.: A Century of physical geography research in the *Annals, Ann. Assoc. Am.*
626 *Geogr.*, 100(5), 1049–1059, 2010.
- 627 Ayala, A., McPhee, J. and Vargas, X.: Altitudinal gradients, midwinter melt, and wind
628 effects on snow accumulation in semiarid midlatitude Andes under La Niña conditions,
629 *Water Resour. Res.*, 2014.
- 630 Bales, R. C., Molotch, N. P., Painter, T. H., Dettinger, M. D., Rice, R. and Dozier, J.:
631 Mountain hydrology of the western United States, *Water Resour. Res.*, 42(8), W08432,
632 doi:10.1029/2005wr004387, 2006.
- 633 Barthel, R.: A call for more fundamental science in regional hydrogeology, *Hydrogeol. J.*,
634 22(3), 507–510, 2014.
- 635 Beven, K.: Towards integrated environmental models of everywhere: uncertainty, data and
636 modelling as a learning process, *Hydrol. Earth Syst. Sci.*, 11(1), 460–467, 2007.
- 637 Beven, K. J.: Preferential flows and travel time distributions: defining adequate hypothesis
638 tests for hydrological process models, *Hydrol. Process.*, 24(12), 1537–1547, 2010.
- 639 Black, P. E.: *Watershed hydrology*, CRC Press, Boca Raton, FL., 1996.
- 640 Blöschl, G.: Scaling in hydrology, *Hydrol. Process.*, 15(4), 709–711, 2001.
- 641 Brocca, L., Melone, F., Moramarco, T. and Morbidelli, R.: Spatial- temporal variability of
642 soil moisture and its estimation across scales, *Water Resour. Res.*, 46(2), 2010.
- 643 Brutsaert, W.: Long-term groundwater storage trends estimated from streamflow records:
644 Climatic perspective, *Water Resour. Res.*, 44(2), W02409, doi:10.1029/2007WR006518,
645 2008.
- 646 Capell, R., Tetzlaff, D., Hartley, A. J. and Soulsby, C.: Linking metrics of hydrological
647 function and transit times to landscape controls in a heterogeneous mesoscale catchment,
648 *Hydrol. Process.*, 26(3), 405–420, 2012.
- 649 Castle, S. L., Thomas, B. F., Reager, J. T., Rodell, M., Swenson, S. C. and Famiglietti, J.
650 S.: Groundwater Depletion During Drought Threatens Future Water Security of the
651 Colorado River Basin, *Geophys. Res. Lett.*, doi:10.1002/2014GL061055, 2014.

- 652 Cayan, D. R.: Interannual Climate Variability and Snowpack in the Western United States,
653 *J. Clim.*, 9(5), 928–948, doi:10.1175/1520-0442(1996)009<0928:ICVASI>2.0.CO;2, 1996.
- 654 Clark, M. P., Kavetski, D. and Fenicia, F.: Pursuing the method of multiple working
655 hypotheses for hydrological modeling, *Water Resour. Res.*, 47(9), 2011.
- 656 Cosgrove, B. A., Lohmann, D., Mitchell, K. E., Houser, P. R., Wood, E. F., Schaake, J. C.,
657 Robock, A., Marshall, C., Sheffield, J. and Duan, Q.: Real-time and retrospective forcing in
658 the North American Land Data Assimilation System (NLDAS) project, *J. Geophys. Res.*,
659 108(D22), 8842, 2003.
- 660 Dozier, J.: Mountain hydrology, snow color, and the fourth paradigm, *Eos, Trans. Am.*
661 *Geophys. Union*, 92(43), 373, doi:10.1029/2011EO430001, 2011.
- 662 Famiglietti, J. S., Lo, M., Ho, S. L., Bethune, J., Anderson, K. J., Syed, T. H., Swenson, S.
663 C., de Linage, C. R. and Rodell, M.: Satellites measure recent rates of groundwater
664 depletion in California’s Central Valley, *Geophys. Res. Lett.*, 38(3), L03403,
665 doi:10.1029/2010gl046442, 2011.
- 666 Famiglietti, J. S. and Rodell, M.: Water in the Balance, *Science* (80-.), 340(6138), 1300–
667 1301, 2013.
- 668 Feng, J., Wang, L. and Chen, W.: How does the East Asian summer monsoon behave in the
669 decaying phase of El Niño during different PDO phases?, *J. Clim.*, 27(7), 2682–2698,
670 2014.
- 671 Gleeson, T., Wada, Y., Bierkens, M. F. P. and van Beek, L. P. H.: Water balance of global
672 aquifers revealed by groundwater footprint, *Nature*, 488(7410), 197–200, 2012.
- 673 Gleick, P.: Water, Drought, Climate Change, and Conflict in Syria, *Weather. Clim. Soc.*, 6,
674 331–340, 2014a.
- 675 Gleick, P. H.: *The World’s Water Volume 8: The Biennial Report on Freshwater*
676 *Resources*, Island Press., 2014b.
- 677 Iizumi, T., Luo, J.-J., Challinor, A. J., Sakurai, G., Yokozawa, M., Sakuma, H., Brown, M.
678 E. and Yamagata, T.: Impacts of El Niño Southern Oscillation on the global yields of major
679 crops, *Nat. Commun.*, 5, 2014.
- 680 Jarvis, W. T.: Unitization: a lesson in collective action from the oil industry for aquifer
681 governance, *Water Int.*, 36(5), 619–630, 2011.
- 682 Jarvis, W. T.: *Contesting Hidden Waters: Conflict Resolution for Groundwater and*
683 *Aquifers*, Routledge., 2014.

- 684 Jefferson, A., Nolin, A., Lewis, S. and Tague, C.: Hydrogeologic controls on streamflow
685 sensitivity to climate variation, *Hydrol. Process.*, 22(22), 4371–4385,
686 doi:10.1002/hyp.7041, 2008.
- 687 Kirchner, J. W.: Catchments as simple dynamical systems: Catchment characterization,
688 rainfall-runoff modeling, and doing hydrology backward, *Water Resour. Res.*, 45(2),
689 W02429, doi:10.1029/2008WR006912, 2009.
- 690 Koster, R. D., Mahanama, S. P. P., Livneh, B., Lettenmaier, D. P. and Reichle, R. H.: Skill
691 in streamflow forecasts derived from large-scale estimates of soil moisture and snow, *Nat.*
692 *Geosci.*, 3(9), 613–616,
693 doi:http://www.nature.com/ngeo/journal/v3/n9/supinfo/ngeo944_S1.html, 2010.
- 694 Landerer, F. W. and Swenson, S. C.: Accuracy of scaled GRACE terrestrial water storage
695 estimates, *Water Resour. Res.*, 48(4), W04531, doi:10.1029/2011wr011453, 2012.
- 696 Legates, D. R. and McCabe, G. J.: Evaluating the use of “goodness-of-fit” measures in
697 hydrologic and hydroclimatic model validation, *Water Resour. Res.*, 35(1), 233–241, 1999.
- 698 Li, B., Rodell, M., Zaitchik, B. F., Reichle, R. H., Koster, R. D. and van Dam, T. M.:
699 Assimilation of GRACE terrestrial water storage into a land surface model: Evaluation and
700 potential value for drought monitoring in western and central Europe, *J. Hydrol.*, 446, 103–
701 115, 2012.
- 702 Mahanama, S., Livneh, B., Koster, R., Lettenmaier, D. and Reichle, R.: Soil Moisture,
703 Snow, and Seasonal Streamflow Forecasts in the United States, *J. Hydrometeorol.*, 13(1),
704 189–203, doi:10.1175/JHM-D-11-046.1, 2011.
- 705 McDonnell, J. J.: Where does water go when it rains? Moving beyond the variable source
706 area concept of rainfall-runoff response, *Hydrol. Process.*, 17(9), 1869–1875,
707 doi:10.1002/hyp.5132, 2003.
- 708 McDonnell, J. J., Sivapalan, M., Vache, K., Dunn, S., Grant, G., Haggerty, R., Hinz, C.,
709 Hooper, R., Kirchner, J., Roderick, M. L., Selker, J. and Weiler, M.: Moving beyond
710 heterogeneity and process complexity: A new vision for watershed hydrology, *Water*
711 *Resour. Res.*, 43(7), doi:10.1029/2006wr005467, 2007.
- 712 McGlynn, B. L. and McDonnell, J. J.: Quantifying the relative contributions of riparian and
713 hillslope zones to catchment runoff, *Water Resour. Res.*, 39(11),
714 doi:10.1029/2003WR002091, 2003.
- 715 McNamara, J. P., Tetzlaff, D., Bishop, K., Soulsby, C., Seyfried, M., Peters, N. E.,
716 Aulenbach, B. T. and Hooper, R.: Storage as a Metric of Catchment Comparison, *Hydrol.*
717 *Process.*, 25(21), 3364–3371, doi:10.1002/hyp.8113, 2011.

- 718 Milly, P. C. D., Betancourt, J., Falkenmark, M., Hirsch, R. M., Kundzewicz, Z. W.,
 719 Lettenmaier, D. P. and Stouffer, R. J.: Stationarity Is Dead: Whither Water Management?,
 720 *Science* (80-.), 319(5863), 573–574, doi:10.1126/science.1151915, 2008.
- 721 Moradkhani, H. and Sorooshian, S.: General Review of Rainfall-Runoff Modeling: Model
 722 Calibration, Data Assimilation, and Uncertainty Analysis, in *Hydrological Modelling and
 723 the Water Cycle*, pp. 1–24., 2008.
- 724 National Operational Hydrologic Remote Sensing Center: Snow Data Assimilation System
 725 (SNODAS) Data Products at NSIDC, [2003-2012], National Snow and Ice Data Center,
 726 Boulder, Colorado USA., 2004.
- 727 Nolin, A. W.: Perspectives on Climate Change, Mountain Hydrology, and Water Resources
 728 in the Oregon Cascades, USA, *Mt. Res. Dev.*, 32(S1), S35–S46, doi:10.1659/mrd-journal-
 729 d-11-00038.s1, 2012.
- 730 Nolin, A. W., Sproles, E. A. and Brown, A.: Climate change impacts on snow and water
 731 resources in the Columbia, Willamette, and McKenzie River Basins, USA: A nested
 732 watershed study. , in *Transboundary River Governance in the Face of Uncertainty: The
 733 Columbia River Treaty*, edited by B. Cosens, Oregon State University Press, Corvallis,
 734 OR., 2012.
- 735 Oregon Water Supply and Conservation Initiative: Southern Willamette valley municipal
 736 water providers final report., 2008.
- 737 Payne, J. T., Wood, A. W., Hamlet, A. F., Palmer, R. N. and Lettenmaier, D. P.: Mitigating
 738 the Effects of Climate Change on the Water Resources of the Columbia River Basin, *Clim.
 739 Change*, 62(1), 233–256, 2004.
- 740 Peel, M. C. and Blöschl, G.: Hydrological modelling in a changing world, *Prog. Phys.
 741 Geogr.*, 35(2), 249–261, 2011.
- 742 Reager, J. T. and Famiglietti, J. S.: Global terrestrial water storage capacity and flood
 743 potential using GRACE, *Geophys. Res. Lett.*, 36(23), L23402, doi:10.1029/2009gl040826,
 744 2009.
- 745 Reager, J. T., Thomas, B. F. and Famiglietti, J. S.: River basin flood potential inferred
 746 using GRACE gravity observations at several months lead time, *Nat. Geosci.*, 7, 588–592,
 747 doi:10.1038/ngeo2203, 2014.
- 748 Riegger, J. and Tourian, M. J.: Characterization of runoff- storage relationships by satellite
 749 gravimetry and remote sensing, *Water Resour. Res.*, 50(4), 3444–3466, 2014.
- 750 Rodell, M., Houser, P. R., Jambor, U., Gottschalck, J., Mitchell, K., Meng, C. J., Arsenault,
 751 K., Cosgrove, B., Radakovich, J., Bosilovich, M., Entin, J. K., Walker, J. P., Lohmann, D.

- 752 and Toll, D.: The Global Land Data Assimilation System, *Bull. Am. Meteorol. Soc.*, 85(3),
753 381–394, doi:10.1175/bams-85-3-381, 2004.
- 754 Rodell, M., Velicogna, I. and Famiglietti, J. S.: Satellite-based estimates of groundwater
755 depletion in India, *Nature*, 460(7258), 999–1002, 2009.
- 756 Rupp, D. E., Abatzoglou, J. T., Hegewisch, K. C. and Mote, P. W.: Evaluation of CMIP5
757 20th century climate simulations for the Pacific Northwest USA, *J. Geophys. Res. Atmos.*,
758 2013.
- 759 Sayama, T., McDonnell, J. J., Dhakal, A. and Sullivan, K.: How much water can a
760 watershed store?, *Hydrol. Process.*, 25(25), 3899–3908, doi:10.1002/hyp.8288, 2011.
- 761 Serreze, M. C., Clark, M. P., Armstrong, R. L., McGinnis, D. A. and Pulwarty, R. S.:
762 Characteristics of the western United States snowpack from snowpack telemetry
763 (SNOTEL) data, *Water Resour. Res.*, 35(7), 2145–2160, doi:10.1029/1999wr900090, 1999.
- 764 Skøien, J. O., Blöschl, G. and Western, A. W.: Characteristic space scales and timescales in
765 hydrology, *Water Resour. Res.*, 39(10), 2003.
- 766 Spence, C.: A paradigm shift in hydrology: Storage thresholds across scales influence
767 catchment runoff generation, *Geogr. Compass*, 4(7), 819–833, 2010.
- 768 Sproles, E. A., Nolin, A. W., Rittger, K. and Painter, T. H.: Climate change impacts on
769 maritime mountain snowpack in the Oregon Cascades, *Hydrol. Earth Syst. Sci.*, 17(7),
770 2581–2597, doi:10.5194/hess-17-2581-2013, 2013.
- 771 Swenson, S. and Wahr, J.: Post-processing removal of correlated errors in GRACE data,
772 *Geophys. Res. Lett.*, 33(8), L08402, doi:10.1029/2005gl025285, 2006.
- 773 Swenson, S., Yeh, P. J. F., Wahr, J. and Famiglietti, J.: A comparison of terrestrial water
774 storage variations from GRACE with in situ measurements from Illinois, *Geophys. Res.*
775 *Lett.*, 33(16), L16401, doi:10.1029/2006gl026962, 2006.
- 776 Tague, C., Grant, G., Farrell, M., Choate, J. and Jefferson, A.: Deep groundwater mediates
777 streamflow response to climate warming in the Oregon Cascades, *Clim. Change*, 86(1),
778 189–210, 2008.
- 779 Tapley, B. D., Bettadpur, S., Ries, J. C., Thompson, P. F. and Watkins, M. M.: GRACE
780 measurements of mass variability in the Earth system, *Science (80-.)*, 305(5683), 503–
781 505, 2004.
- 782 The MathWorks: MATLAB and Statistics Toolbox Release 2013a, 2013.

- 783 Thompson, S. E., Harman, C. J., Schumer, R., Wilson, J. S., Basu, N. B., Brooks, P. D.,
784 Donner, S. D., Hassan, M. A., Packman, A. I. and Rao, P. S. C.: Patterns, puzzles and
785 people: implementing hydrologic synthesis, *Hydrol. Process.*, 25(20), 3256–3266, 2011.
- 786 United States Army Corps of Engineers: Comprehensive water supply study - An
787 examination of current water supply issues, edited by T. M. Hillyer., 2001.
- 788 Voss, K. A., Famiglietti, J. S., Lo, M., Linage, C., Rodell, M. and Swenson, S. C.:
789 Groundwater depletion in the Middle East from GRACE with implications for
790 transboundary water management in the Tigris- Euphrates- Western Iran region, *Water*
791 *Resour. Res.*, 2013.
- 792 Wagener, T., Sivapalan, M., Troch, P. A., McGlynn, B. L., Harman, C. J., Gupta, H. V,
793 Kumar, P., Rao, P. S. C., Basu, N. B. and Wilson, J. S.: The future of hydrology: An
794 evolving science for a changing world, *Water Resour. Res.*, 46(5), 2010.
- 795 Wagener, T., Sivapalan, M., Troch, P. and Woods, R.: Catchment classification and
796 hydrologic similarity, *Geogr. Compass*, 1(4), 901–931, doi:10.1111/j.1749-
797 8198.2007.00039.x, 2007.
- 798 Wahr, J., Swenson, S. and Velicogna, I.: Accuracy of GRACE mass estimates, *Geophys.*
799 *Res. Lett.*, 33(6), L06401, doi:10.1029/2005gl025305, 2006.
- 800 Webster, C. S., Kingston, D. G. and Kerr, T.: Inter- annual variation in the topographic
801 controls on catchment- scale snow distribution in a maritime alpine catchment, New
802 Zealand, *Hydrol. Process.*, 2014.
- 803 Western, A. W., Grayson, R. B. and Blöschl, G.: Scaling of soil moisture: A hydrologic
804 perspective, *Annu. Rev. Earth Planet. Sci.*, 30(1), 149–180, 2002.
- 805 Wu, H., Kimball, J. S., Elsner, M. M., Mantua, N., Adler, R. F. and Stanford, J.: Projected
806 climate change impacts on the hydrology and temperature of Pacific Northwest rivers,
807 *Water Resour. Res.*, 48(11), W11530, doi:10.1029/2012wr012082, 2012.
- 808 Yeh, P. J. F., Swenson, S. C., Famiglietti, J. S. and Rodell, M.: Remote sensing of
809 groundwater storage changes in Illinois using the Gravity Recovery and Climate
810 Experiment (GRACE), *Water Resour. Res.*, 42(12), W12203, doi:10.1029/2006wr005374,
811 2006.
- 812 Zaitchik, B. F., Rodell, M. and Reichle, R. H.: Assimilation of GRACE terrestrial water
813 storage data into a land surface model: Results for the Mississippi River Basin, *J.*
814 *Hydrometeorol.*, 9(3), 535–548, doi:10.1175/2007JHM951.1, 2008.
- 815 Zang, C. F., Liu, J., Velde, M. and Kraxner, F.: Assessment of spatial and temporal patterns
816 of green and blue water flows under natural conditions in inland river basins in Northwest
817 China, *Hydrol. Earth Syst. Sci.*, 16(8), 2859–2870, 2012.

Table 1: Comparison of performance metrics using the dual-pass approach to apply GRACE TWSA data, model derived snow (SWE), and soil moisture (SM) products in predicting seasonal (R_{season}) and August (R_{Aug}) runoff by watershed. Average values for the three basins are also provided. RMSE values are in mm. Complete results can be found in Appendix table A3.

	Upper Columbia							
	R_{season}				R_{Aug}			
	$TWSA_{\text{Mar}}$	$TWSA_{\text{Apr}}$	SWE_{Mar}	SM_{Mar}	$TWSA_{\text{Mar}}$	$TWSA_{\text{Apr}}$	SWE_{Mar}	SM_{Mar}
NSE	0.82	0.87	0.46	< 0	0.71	0.70	< 0	< 0
RMSE	33.06	27.62	56.10	> 1000	5.71	5.38	13.08	143.17
R^2	0.86	0.88	0.58	0.00	0.71	0.71	0.28	0.05
	Snake River							
NSE	0.46	0.29	< 0	0.85	< 0	< 0	< 0	< 0
RMSE	14.03	15.71	21.53	7.38	13.59	0.76	0.78	0.72
R^2	0.59	0.47	0.08	0.86	0.15	0.08	0.27	0.29
	The Dalles							
NSE	0.98	0.54	0.24	< 0	0.80	0.29	< 0	< 0
RMSE	6.01	26.50	26.48	122.88	1.86	3.31	18.91	22.10
R^2	0.98	0.71	0.39	0.00	0.82	0.71	0.03	0.02
	Average							
NSE	0.75	0.57	0.35	0.85	0.76	0.50	< 0	< 0
RMSE	17.70	23.28	34.70	65.13	7.05	3.15	10.92	55.33
R^2	0.81	0.69	0.35	0.29	0.56	0.50	0.19	0.12

Table 2: Comparison of performance metrics from applying all nine water years of GRACE TWSA data, model derived snow (SWE), and soil moisture (SM) products in predicting seasonal (R_{season}) and August (R_{Aug}) runoff by watershed. Average values for the three basins are also provided. RMSE values are in mm. R^2 values are the same as NSE for this linear regression. Complete results can be found in Appendix table A4.

Upper Columbia								
	R_{season}				R_{Aug}			
	$TWSA_{\text{Mar}}$	$TWSA_{\text{Apr}}$	SWE_{Mar}	SM_{Mar}	$TWSA_{\text{Mar}}$	$TWSA_{\text{Apr}}$	SWE_{Mar}	SM_{Mar}
NSE	0.93	0.92	0.82	0.03	0.76	0.73	0.56	0.09
RMSE	22.18	23.18	36.19	82.90	6.60	6.90	8.92	12.79
Snake River								
NSE	0.83	0.75	0.34	0.93	0.68	0.52	0.62	0.76
RMSE	8.76	10.55	17.23	5.80	0.43	0.52	0.47	0.37
The Dalles								
NSE	0.98	0.91	0.67	0.00	0.88	0.91	0.46	0.02
RMSE	6.22	13.00	24.60	42.67	1.55	1.30	3.30	4.40
Average								
NSE	0.91	0.86	0.61	0.32	0.77	0.72	0.55	0.29
RMSE	12.39	15.58	26.01	43.79	2.86	2.91	4.23	5.85

Table 3: Parameters from the power function curves in each of the three watersheds using TWSA to predict streamflow. Figure 7 provides these results visually.

	Upper Columbia		Snake River		The Dalles	
	$TWSA_{\text{Mar}}$	$TWSA_{\text{Mar}}$	$TWSA_{\text{Mar}}$	$TWSA_{\text{Mar}}$	$TWSA_{\text{Mar}}$	$TWSA_{\text{Mar}}$
	R_{season}	R_{Aug}	R_{season}	R_{Aug}	R_{season}	R_{Aug}
a	2.12E-10	4.83E-06	5.69E-05	2.26E-04	7.40E-10	3.61E-15
b	4.99	3.41	2.88	1.89	5.25	7.28
c	41.06	273.99	23.97	3.30	124.21	15.54

Table A1: The reservoirs used in the GRACE analysis.

Reservoir Name	Operating Agency	Normal Operating Capacity (m³)
Grand Coulee	US Department of Interior	1.16 x 10 ¹⁰
Libby	US Army Corps of Engineers	7.17 x 10 ⁹
Hungry Horse	US Department of Interior	4.28 x 10 ⁹
Dworsha	US Army Corps of Engineers	4.26 x 10 ⁹
American Falls	US Department of Interior	2.10 x 10 ⁹

Table A2: The groundwater wells used in the analysis that compares GRACE-derived groundwater with location-specific wells. USGS is the United States Geological Survey and IDWR is the Idaho Department of Water Resources.

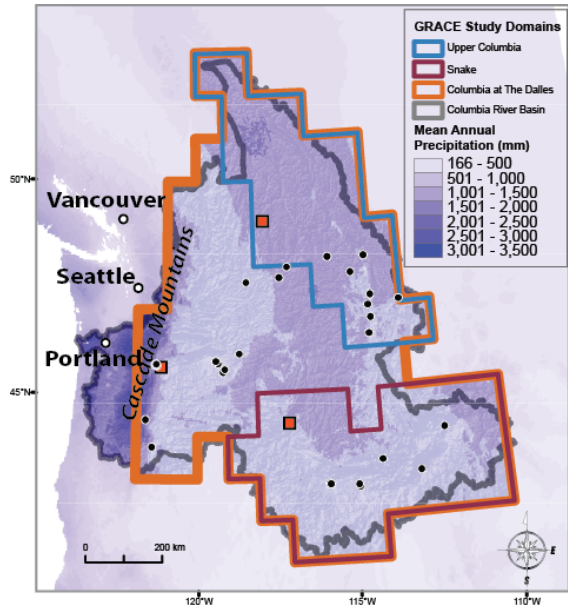
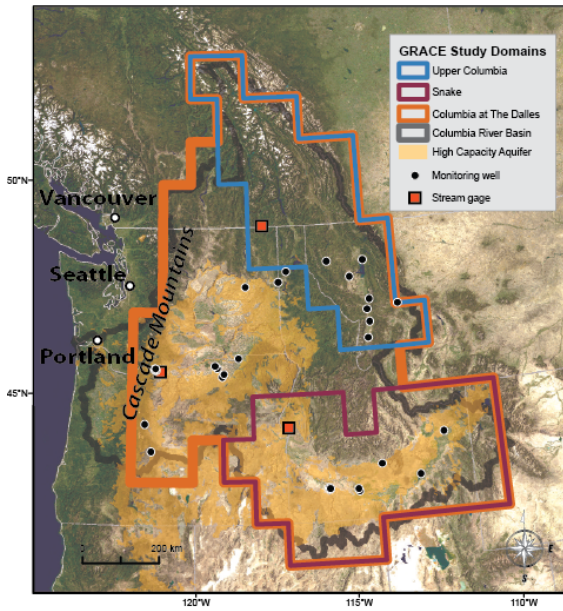
Well Number	Operating Agency
434400121275801	USGS
442242121405501	USGS
452855119064701	USGS
453239119031501	USGS
453845121191401	USGS
453937121215801	USGS
453944121211301	USGS
454013121225901	USGS
454027121212501	USGS
454040121222901	USGS
454047121203701	USGS
454100119164801	USGS
454416119212801	USGS
455418118333001	USGS
461518114090802	USGS
463750114033001	USGS
465520114074001	USGS
470049113035401	USGS
470946114013201	USGS
473442118162201	USGS
474011117072901	USGS
474251114385201	USGS
475439116503401	USGS
480519114091001	USGS
480621115244901	USGS
02S20E-01ACC2	IDWR
07S06E-29BBA1	IDWR
08S06E-03BDC1	IDWR
07S06E-34BCA1	IDWR
09S14E-03BAA1	IDWR
08S14E-16CBB1	IDWR
05S31E-27ABA1	IDWR
07N38E-23DBA1	IDWR

Table A3: Comparison of performance metrics using the dual-pass approach to apply GRACE TWSA, model derived snow (SWE), soil moisture (SM), and subsurface (TWSA_{sub}) data in predicting seasonal (R_{season}) and August (R_{Aug}) runoff by watershed. RMSE values are in mm.

	TWSA			SM			SWE			TWSA _{sub}					
	Feb	Mar	Apr	Feb	Mar	Apr	Feb	Mar	Apr	Feb	Mar	Apr			
Upper Columbia	R_{season}	NSE	< 0	0.82	0.87	< 0	< 0	< 0	< 0	0.46	< 0	< 0	< 0	< 0	< 0
		RMSE	84	33	28	>1000	>1000	134	110	56	309	>1000	>1000	354	
		R ²	0.43	0.86	0.88	0.01	0.00	0.07	0.23	0.58	0.27	0.15	0.02	0.02	
	R_{July}	NSE	< 0	0.90	0.84	< 0	< 0	< 0	< 0	< 0	< 0	< 0	< 0	< 0	
		RMSE	32	7	8	>1000	71	56	28	25	108	>1000	>1000	123	
		R ²	0.19	0.93	0.92	0.01	0.00	0.00	0.32	0.45	0.24	0.05	0.01	0.01	
	R_{Aug}	NSE	< 0	0.71	0.70	< 0	< 0	< 0	< 0	< 0	< 0	< 0	< 0	< 0	
		RMSE	228	6	5	>1000	143	32	12	13	51	>1000	>1000	30	
		R ²	0.19	0.71	0.71	0.07	0.05	0.30	0.25	0.28	0.12	0.18	0.11	0.01	
	R_{Sept}	NSE	< 0	< 0	< 0	< 0	< 0	< 0	< 0	< 0	< 0	< 0	< 0	< 0	
		RMSE	2	21	104	4	28	10	>1000	3	50	20	587	6	
		R ²	0.12	0.06	0.12	0.09	0.24	0.20	0.04	0.07	0.04	0.04	0.02	0.03	
Snake River	R_{season}	NSE	< 0	0.46	0.29	0.58	0.85	< 0	< 0	< 0	0.09	< 0	< 0	< 0	
		RMSE	258	14	16	12	7	52	5	22	8	>1000	108	474	
		R ²	0.21	0.59	0.47	0.64	0.86	0.29	0.00	0.08	0.13	0.04	0.11	0.01	
	R_{July}	NSE	< 0	< 0	< 0	< 0	< 0	< 0	< 0	< 0	< 0	< 0	< 0	< 0	
		RMSE	23	3	2	2	2	40	1	2	1	99	>1000	35	
		R ²	0.00	0.05	0.01	0.01	0.09	0.11	0.15	0.00	0.04	0.00	0.06	0.02	
	R_{Aug}	NSE	< 0	< 0	-0.70	< 0	< 0	< 0	< 0	< 0	0.65	< 0	< 0	< 0	
		RMSE	11	13.59	0.76	1	1	2	0	1	1	>1000	>1000	474	
		R ²	0.05	0.15	0.08	0.06	0.29	0.10	0.00	0.27	0.67	0.04	0.11	0.01	
	R_{Sept}	NSE	< 0	< 0	-0.94	< 0	< 0	< 0	< 0	< 0	0.03	< 0	< 0	< 0	
		RMSE	16	1	1	1	1	1	0	1	0	140	8	435	
		R ²	0.01	0.04	0.03	0.07	0.15	0.11	0.03	0.00	0.11	0.00	0.00	0.01	
The Dalles	R_{season}	NSE	< 0	0.98	0.54	< 0	< 0	< 0	0.24	0.14	< 0	< 0	< 0		
		RMSE	84	61	27	267	122	363	>1000	26	26	13	5231	737	
		R ²	0.20	0.98	0.71	0.01	0.00	0.02	0.13	0.39	0.29	0.02	0.00	0.00	
	R_{July}	NSE	< 0	0.86	< 0	< 0	< 0	< 0	< 0	0.28	< 0	< 0	< 0	< 0	
		RMSE	19	3	10	>1000	16	80	>1000	4	6	4	4	311	
		R ²	0.05	0.86	0.64	0.00	0.00	0.02	0.03	0.30	0.10	0.00	0.00	0.00	
	R_{Aug}	NSE	< 0	0.80	0.29	< 0	< 0	< 0	< 0	< 0	0.05	< 0	< 0	< 0	
		RMSE	9	2	3	>1000	22	16	>1000	19	2	2	1	3	
		R ²	0.04	0.82	0.71	0.04	0.02	0.00	0.02	0.03	0.12	0.00	0.00	0.12	
	R_{Sept}	NSE	< 0	0.41	< 0	< 0	< 0	< 0	< 0	< 0	< 0	< 0	0.05	< 0	
		RMSE	5	1	3	756	3	7	1	5x10 ⁹	7x10 ¹⁰	6	1	2	
		R ²	0.00	0.42	0.28	0.03	0.01	0.03	0.06	0.02	0.02	0.22	0.06	0.14	

Table A4: Comparison of performance metrics from applying all nine water years of GRACE TWSA, model derived snow (SWE), soil moisture (SM), and subsurface (TWSA_{sub}) data in predicting seasonal (R_{season}) and August (R_{Aug}) runoff by watershed. RMSE values are in mm. R^2 values are the same as NSE for this linear regression.

		TWSA			SM			SWE			TWSA _{sub}				
		Feb	Mar	Apr	Feb	Mar	Apr	Feb	Mar	Apr	Feb	Mar	Apr		
Upper Columbia	R_{season}	NSE	0.84	0.93	0.92	0.01	0.03	0.33	0.63	0.82	0.62	0.15	0.22	0.22	
		RMSE	28.62	19.81	20.72	8.38	14.30	36.80	37.78	30.27	37.85	28.22	32.50	32.50	
	R_{July}	NSE	0.75	0.95	0.96	0.01	0.00	0.18	0.53	0.79	0.60	0.05	0.22	0.22	
		RMSE	10.38	5.00	4.74	2.16	1.34	9.10	11.95	9.80	11.73	5.38	9.86	9.86	
	R_{Aug}	NSE	0.62	0.76	0.73	0.07	0.09	0.44	0.37	0.56	0.34	0.18	0.11	0.23	
		RMSE	6.02	5.31	5.48	3.12	3.50	6.15	6.00	6.16	5.87	4.80	3.95	5.22	
	R_{Sept}	NSE	0.20	0.07	0.13	0.31	0.28	0.40	0.04	0.04	0.10	0.39	0.15	0.51	
		RMSE	1.60	1.05	1.32	1.85	1.80	1.96	0.80	0.80	1.22	1.95	1.42	2.00	
	Snake River	R_{season}	NSE	0.39	0.83	0.75	0.84	0.93	0.91	0.09	0.34	0.60	0.35	0.39	0.42
			RMSE	9.59	7.39	8.48	7.15	5.16	5.64	5.60	9.37	9.65	9.39	9.63	9.71
		R_{July}	NSE	0.07	0.43	0.43	0.41	0.63	0.51	0.09	0.21	0.70	0.05	0.19	0.23
			RMSE	0.41	0.80	0.80	0.79	0.78	0.81	0.46	0.66	0.74	0.34	0.63	0.68
R_{Aug}		NSE	0.35	0.68	0.52	0.56	0.76	0.61	0.24	0.62	0.91	0.13	0.09	0.12	
		RMSE	0.34	0.33	0.35	0.35	0.30	0.34	0.30	0.34	0.21	0.24	0.20	0.22	
R_{Sept}		NSE	0.18	0.53	0.58	0.60	0.88	0.66	0.08	0.30	0.91	0.16	0.18	0.18	
		RMSE	0.34	0.44	0.44	0.43	0.29	0.42	0.25	0.41	0.25	0.32	0.34	0.34	
The Dalles		R_{season}	NSE	0.48	0.98	0.91	0.00	0.01	0.22	0.21	0.67	0.65	0.19	0.23	0.27
			RMSE	19.82	5.70	11.43	2.10	3.59	16.53	16.06	18.65	18.95	15.43	16.74	17.61
		R_{July}	NSE	0.27	0.89	0.89	0.04	0.03	0.09	0.07	0.52	0.51	0.20	0.38	0.40
			RMSE	4.05	2.90	2.87	1.73	1.52	2.64	2.27	4.55	4.55	3.66	4.43	4.47
	R_{Aug}	NSE	0.29	0.88	0.91	0.04	0.02	0.24	0.05	0.45	0.42	0.34	0.44	0.49	
		RMSE	1.89	1.34	1.22	0.77	0.65	1.78	0.88	2.07	2.05	1.96	2.06	2.08	
	R_{Sept}	NSE	0.20	0.57	0.53	0.03	0.03	0.13	0.02	0.29	0.34	0.37	0.15	0.35	
		RMSE	0.75	0.94	0.94	0.34	0.31	0.63	0.28	0.86	0.90	0.92	0.67	0.90	



Watershed

Physical Characteristics

Climate

Upper Columbia
(155,000 km²)

- Steep topography
- Low aquifer storage
- Responsive runoff

Wet maritime conditions with 900 mm of annual precipitation, and substantial snowpack accumulation

Snake River
(182,000 km²)

- Low relief topography
- High aquifer storage
- Muted runoff

Dry continental climate with 350 mm of annual precipitation, falling primarily at upper elevations as snow

The Dalles
(614,000 km²)

- Includes the Upper Columbia and Snake River
- Topography is a blend of the Upper Columbia and Snake River
- High storage capacity
- Large system that floods

Mix of dry continental climate plains and wet uplands. Mean annual precipitation is 625 mm, with considerable snowpack accumulation in the mountains

Fig. 1: Context map and descriptions of the three study watersheds and the locations of the groundwater wells used in the study.

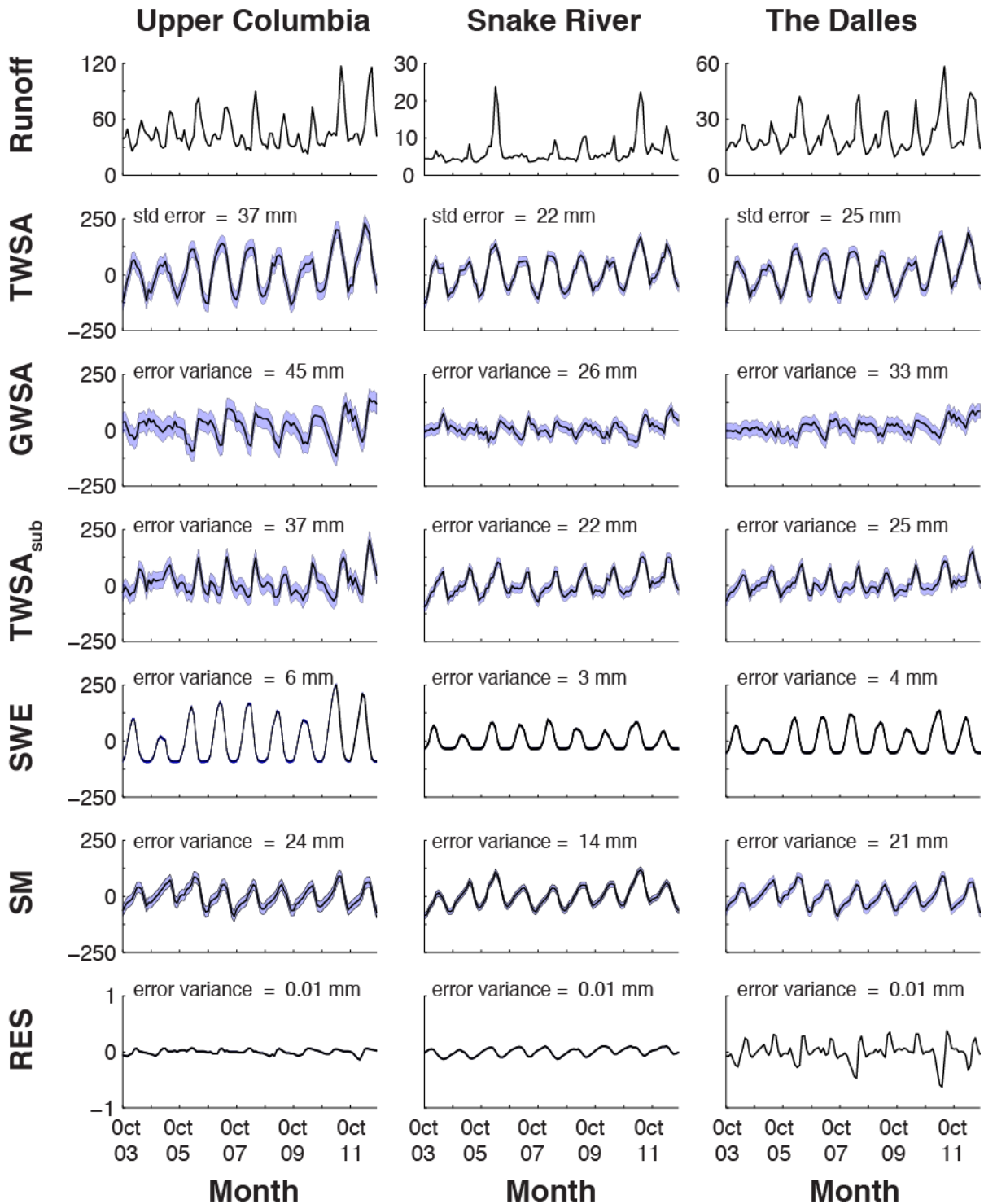


Fig. 2 Monthly storage anomalies for Runoff, TWSA, and the subcomponents of terrestrial water for the three watersheds. Standard errors and error variance for hydrological component are noted in each sub-figure, and represented by the blue shading. All units on the vertical axis are in mm. Note the different vertical scales for Runoff.

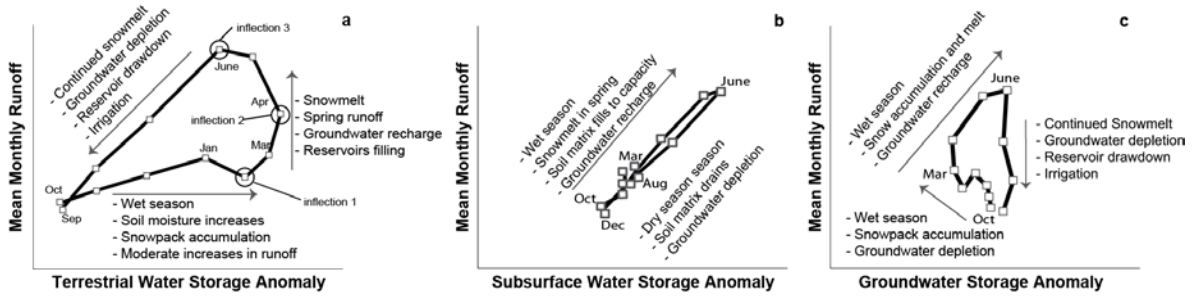


Fig. 3a-c: Annotated hysteresis curves of terrestrial water storage anomalies (a), the subsurface water storage anomalies ($TWSA_{sub}$; b), and groundwater storage anomalies (c) based upon the nine-year mean for the Columbia River at The Dalles. These curves describe the fluxes of water moving through the watershed.

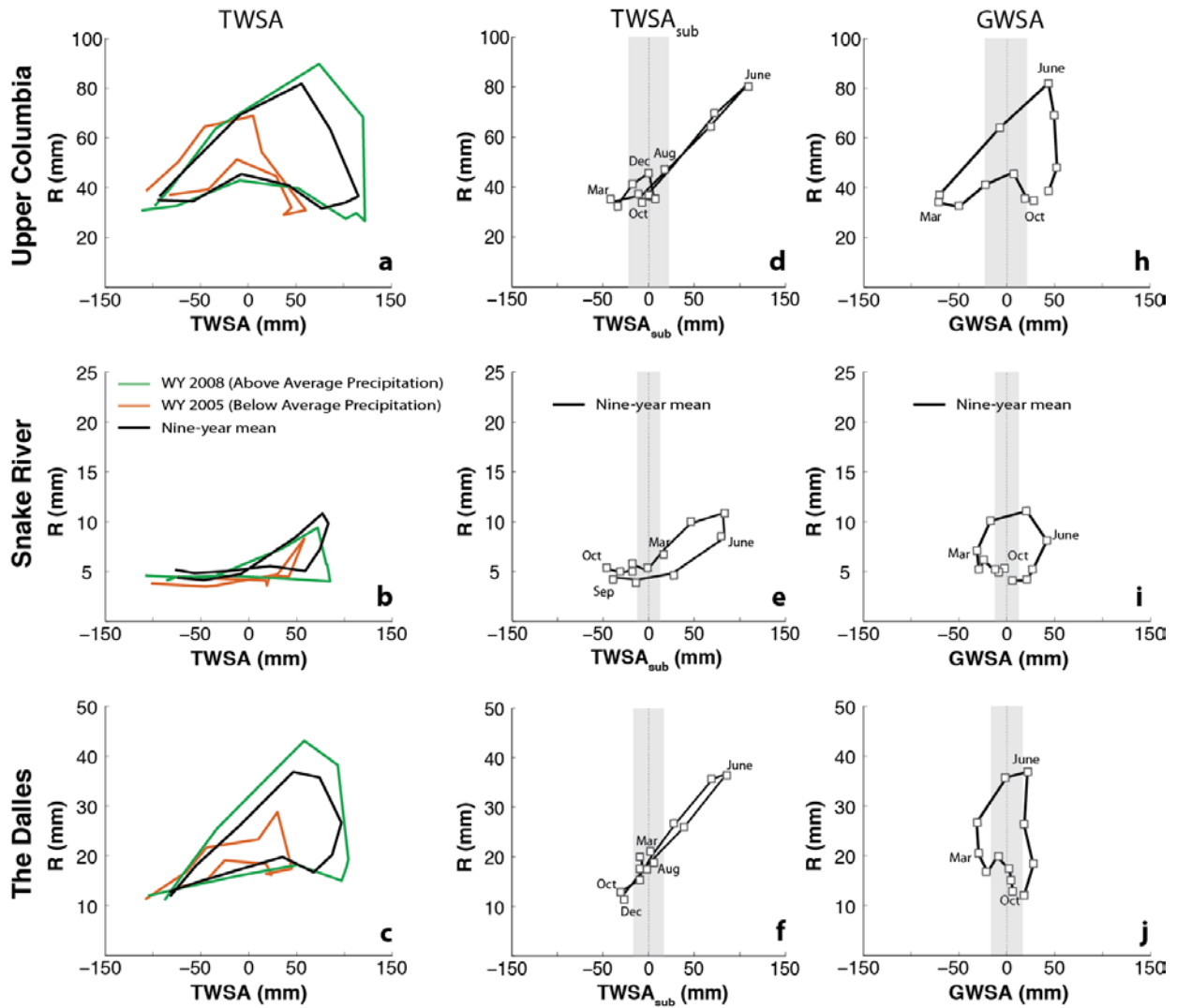


Fig. 4a-f: Individual hysteresis curves for the three study watersheds for $TWSA$ (a-c), $TWSA_{sub}$ (d-f), and $GWSA$ (h-j). $TWSA_{sub}$ in the Upper Columbia and The Dalles collapses to represent a shape more commonly associated with the hysteresis of a soil matrix. The Snake River retains a similar looping shape. The grey areas in the $TWSA_{sub}$ and $GWSA$ plots provide a visual reference of the $TWSA$ error variance for each watershed. The low topography and high storage capacity of the Snake aquifer provides a consistent groundwater signal, as compared to the limited aquifer of the Upper Columbia, which fills and drains quickly. Note the different scales on the y-axes.

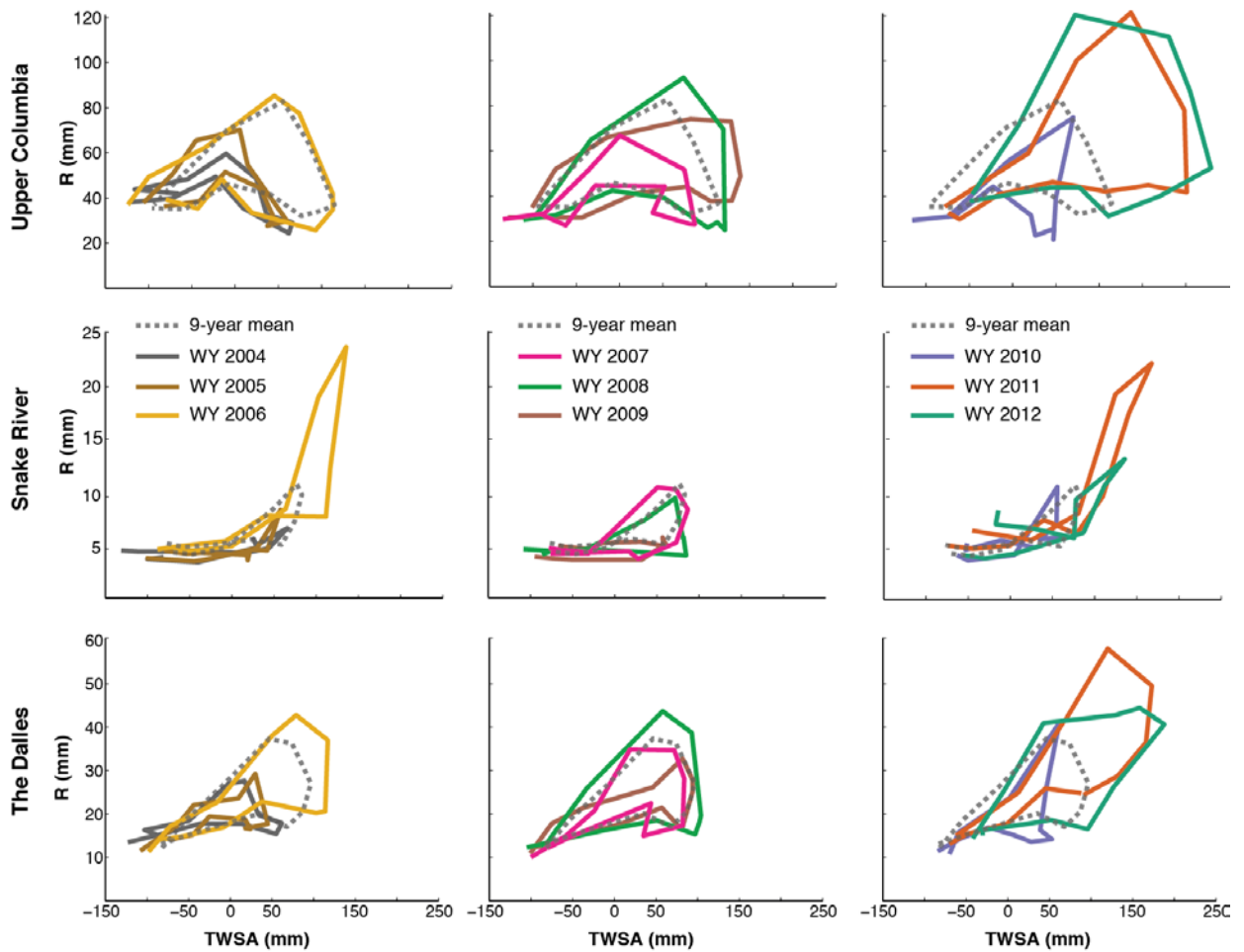


Fig. 5: Plots of the hysteresis curves for $TWSA$ in each of the three study watersheds across all nine water years. For visual clarity, each plot contains three water years and the nine-year mean. Note the different scales on the y-axes for each basin.

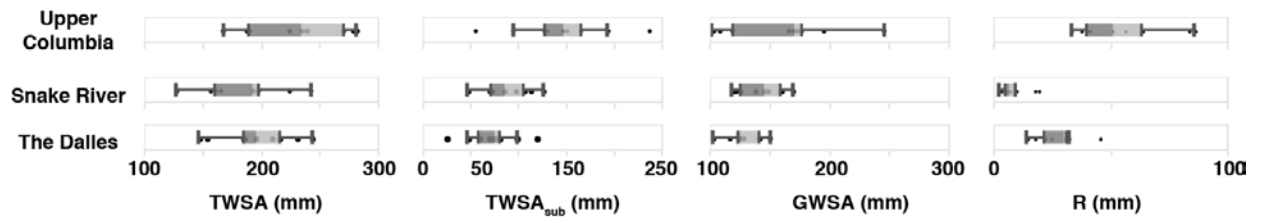


Fig. 6: The intra-annual range of $TWSA$, $TWSA_{sub}$, $GWSA$, and R for the nine water years of the study period.

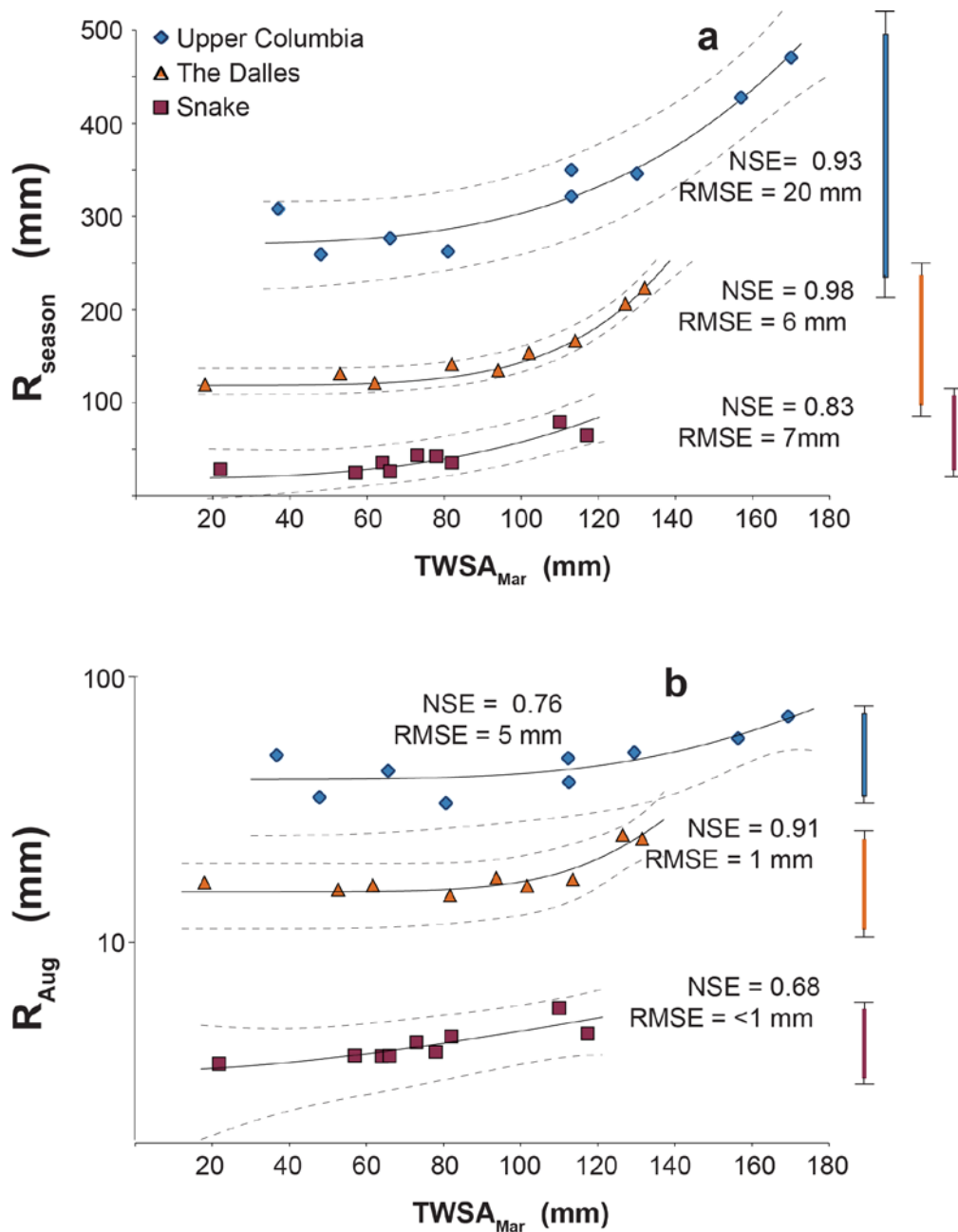


Fig. 7a-b: Measurements of terrestrial water storage anomalies in March ($TWSA_{Mar}$) effectively predict the cumulative runoff for April – September (R_{season} ; a), and help describe how these three regional watersheds function as simple non-linear systems. $TWSA_{Mar}$ also predicts mean runoff for August (R_{Aug} ; b), one of the driest months of the year when demand for water is at its peak. The hashed lines represent the 95% confidence intervals. The box plots to the right of each plot represent the range of R for the respective watershed from WY's 1969 – 2012. Note the semi-log y-axis on (b). For complete results and parameters from the empirical model please refer to Tables 1, 2, 3, A3, and A4.